The Influence of Speckle Statistics on Contrast Metrics in Ultrasound Imaging

Stine M. Hverven*, Ole Marius Hoel Rindal*, Alfonso Rodriguez-Molares† and Andreas Austeng*
*Department of Informatics
University of Oslo
Oslo, Norway
Email: stinemhv@ifi.uio.no
†Department of Circulation and Medical Imaging
Norwegian University of Science and Technology
Trondheim, Norway

***Abstract*—Adaptive beamformers aim for improved resolution and contrast in the ultrasound images, and their performance is typically benchmarked using metrics such as contrast ratio (CR) and contrast-to-noise ratio (CNR). Using synthetic aperture Field II simulations, we show that certain beamformers alter speckle statistics and that this opens up for cherry picking of contrast metrics.**

***Keywords*—Adaptive beamforming, Contrast metrics, Speckle statistics, Contrast-to-noise ratio, Ultrasound.**

I. Introduction

Quality assessment of ultrasound images is difficult since image quality is subjective to the human observer. Nevertheless, image quality metrics are imperative when benchmarking different beamforming techniques. If we do not know how a beamformer alters an image, a quality metric might give an incorrect measurement of the actual image quality. Using the standard Delay-And-Sum (DAS) beamformer as a reference, we examine several adaptive beamformers presented in literature; Capons Minimum Variance (MV), Eigenspace Based Minimum Variance (EBMV), Coherence Factor (CF), Generalized Coherence Factor (GCF), Phase Coherence Factor (PCF) and Delay-Multiply-And-Sum (DMAS). We show that the speckle statistics for some of these adaptive beamformers are dependent on both scattering intensity and location of the region of interest, resulting in contradicting measurements of standard contrast metrics.

II. Background

In this section we briefly introduce the theory for the following beamforming methods; DAS, MV, EBMV, CF, GCF, PCF and DMAS. We refer to [1] and [2] for full description of the implementation of the beamformers and the parameters used in this study.

A. Conventional Delay-And-Sum (DAS)

Conventional DAS for image pixel $[z, x]$ is defined as:

$$S_{\text{DAS}}[z,x] = \sum_{m=0}^{M-1} w_m y_m[z,x] \tag{1}$$

where M is the number of elements, $y_m[z,x]$ is the delayed signal received at element m, and w_m is a predefined weight for element m.

B. Minimum Variance Beamforming

Capon's Minimum Variance (MV) beamformer calculates for each pixel a data dependent set of weights $w^T = \{w_0, w_1, \ldots, w_{M-1}\}$ that minimizes power while maintaining unity gain in the steering direction [3]. The solution found with Lagrange multipliers turns out to be dependent on the spatial covariance matrix. The MV weights are used in the summation in (1).

The Eigenspace Based Minimum Variance (EBMV) beamformer is an extension of the MV beamformer which utilizes the eigenstructure of the covariance matrix to enhance performance [4]. The covariance matrix is eigendecomposed into a signal and noise subspace, and the conventional MV weights are projected onto the signal subspace.

C. Coherence Based Beamforming

The Coherence Factor (CF) beamformer calculates the ratio between coherent and incoherent energy across the aperture [5]. It is used as an adaptive weight to the DAS image [6].

The Generalized Coherence Factor (GCF) beamformer is an extension of CF which utilizes the Fourier-spectrum over the receive aperture of the delayed channel data [6]. The GCF is calculated as the ratio between the energy in a small angular sector around the direction of interest divided by the total energy of the Fourier-spectrum. It is also used as an adaptive weight to the DAS image.

The Phase Coherence Factor (PCF) beamformer [7] calculates for each pixel an adaptive weight based on the phase of the receive data. The weights are multiplied with the DAS image.

The Delay-Multiply-And-Sum (DMAS) [8] multiplies the delayed RF-signals using a "signed" square root. The sum of these signals is band-pass filtered around an "artificial second harmonic" signal before conventional envelope detection and log-compression of the signal results in the final image. It is not obvious that this is a "coherence based beamformer". However, it has been shown that "The DMAS enhances signal coherence and can be seen as an intermediate solution between the DAS beamformer and the coherence factor method" [9].

III. Methods

Synthetic transmit aperture datasets were simulated in Field II [10][11] using a 128 element, λ pitch, linear array with 5 MHz center frequency (L11-4v). The simulated phantom

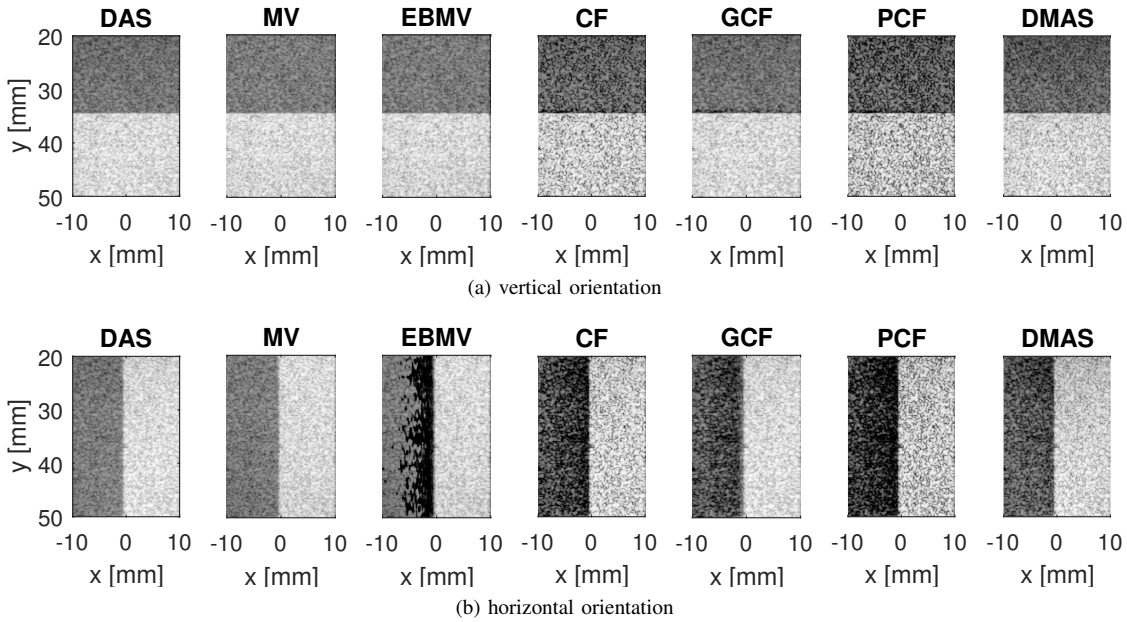

(a) vertical orientation

(b) horizontal orientation

Fig. 1. Ultrasound images for the seven different beamformers. The vertical orientation of the speckle phantom is in (a), and the horizontal orientation is in (b). The images are shown with a dynamic range of 80 dB.

consists of two speckle regions with intensity at -30 dB and 0 dB, using at least 43 scatterers per resolution cell. To investigate any spatial dependency of the beamformer's speckle statistics, two different phantoms were designed. The first phantom has the speckle regions in vertical orientation, where the low intensity region is above the high intensity region as shown in Fig. 1a. The other phantom is horizontally oriented with the speckle regions located side-by-side as shown in Fig. 1b.

The beamforming was performed in MATLAB (Mathworks, Natick, MA) using The UltraSound ToolBox (USTB) [12]. Each transmit sequence was combined before applying the different beamforming methods briefly described above on the combined receive aperture.

The two most common contrast metrics are contrast ratio (CR) and contrast-to-noise ratio (CNR). CR is defined as [13]:

$$\text{CR} = 20\log_{10}\left(\frac{\mu_1}{\mu_2}\right),$$

where μ_1 and μ_2 are the mean intensity values of the two rectangular speckle regions. The values for the region are calculated with a 0.9 mm margin from the other speckle region, and horizontal and vertical edge margins of 1.5 mm and 3.0 mm. CNR weighs the intensity difference between the two regions with the average variance [14]:

$$\text{CNR} = \frac{|\mu_1 - \mu_2|}{\sqrt{(\sigma_1^2 + \sigma_2^2)/2}},$$

where μ_i is the mean intensity value and σ_i^2 is the variance of speckle region i.

IV. Results

Images created with the DAS, MV, EBMV, CF, GCF, PCF and DMAS beamformers for the vertical speckle phantom are shown in Fig. 1a and images for the horizontal phantom are shown in Fig. 1b. To measure the speckle statistics for the different beamformers in Fig. 1, the normalized probability distribution function (PDF) of each speckle region was estimated. Fig. 2 shows the estimated PDFs of the horizontally oriented phantom shown in Fig. 1, together with the corresponding signal-to-noise ratio (SNR=μ/σ). The estimated PDFs of the speckle region with high intensity is presented in Fig. 2a. The theoretical Rayleigh distribution for DAS, with SNR = 1.91 [15], is plotted for comparison. Fig. 2b presents the statistics of the low intensity speckle region.

Fig. 3 shows the estimated PDFs of the images after log-compression of the intensity values. Fig. 3a shows the vertical speckle phantom and Fig. 3b shows for the horizontal speckle phantom. In both plots the estimated PDFs of the low intensity regions are plotted with a solid line, while the estimated PDFs of the high intensity regions are plotted with a dashed line. The SNR, measured from the envelope before log-compression, is indicated in the legend. Fig. 4 shows the CR and CNR measurements for both phantom orientations for the different beamformers.

V. Discussion

Fig. 1 shows the different beamformed images for our simulation with 30 dB intensity difference between the speckle regions and two phantom orientations. From the images, we notice how especially the CF and PCF images have higher variance than the DAS image. When the two speckle regions are side-by-side , i.e. horizontally oriented, the adaptive beamformers EBMV, CF and PCF seem to darken the low intensity speckle region in the transition between the two regions.

We can observe in Fig. 2a that DAS, MV, EBMV and GCF seem to approximately follow the theoretical Rayleigh distribution. The above beamformers have SNR values close to theoretical Rayleigh, i.e. SNR ≈ 1.91, whereas the CF, PCF and DMAS beamformers have very different distributions and

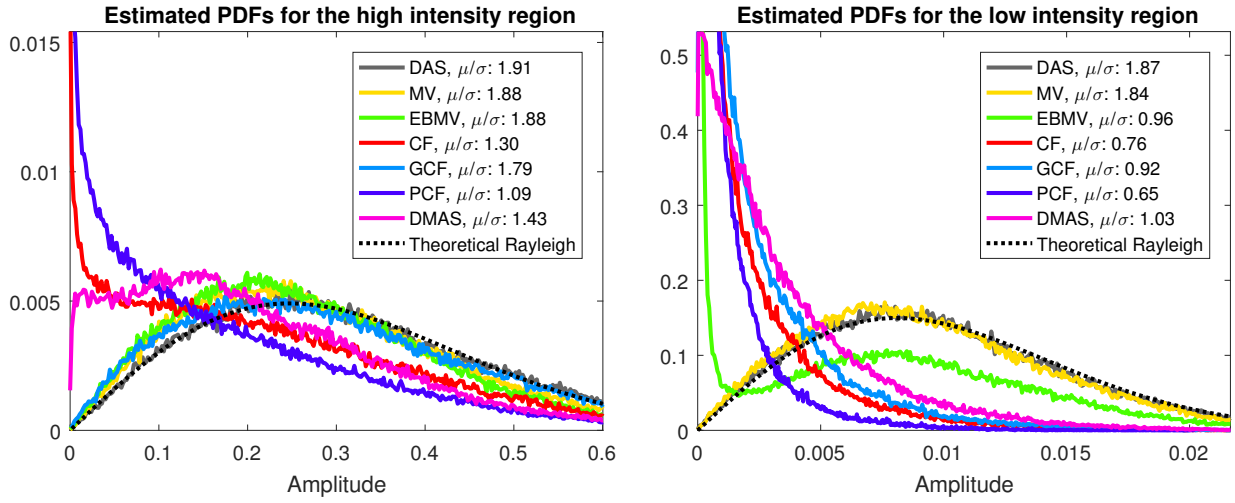

(a) (b)

Fig. 2. Estimated probability distributions (PDF) of the two speckle regions in the horizontal phantom orientation, shown for all beamformers. DAS is compared to its respective theoretical Rayleigh distribution.

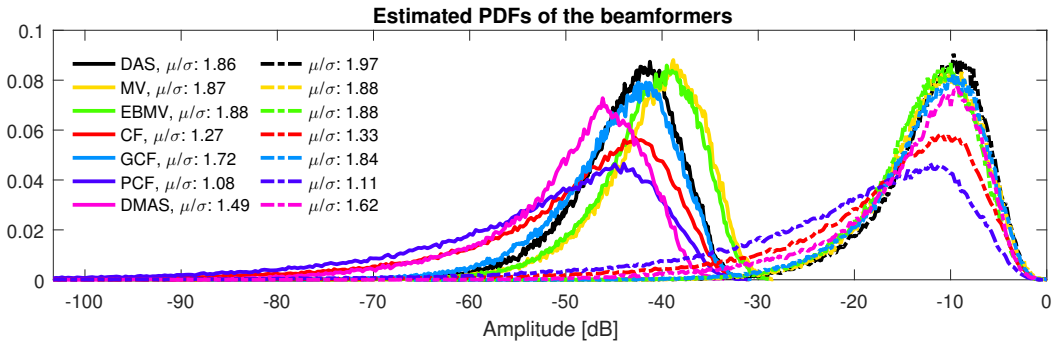

(a) Estimated PDF of dB-scaled image data, vertical orientation

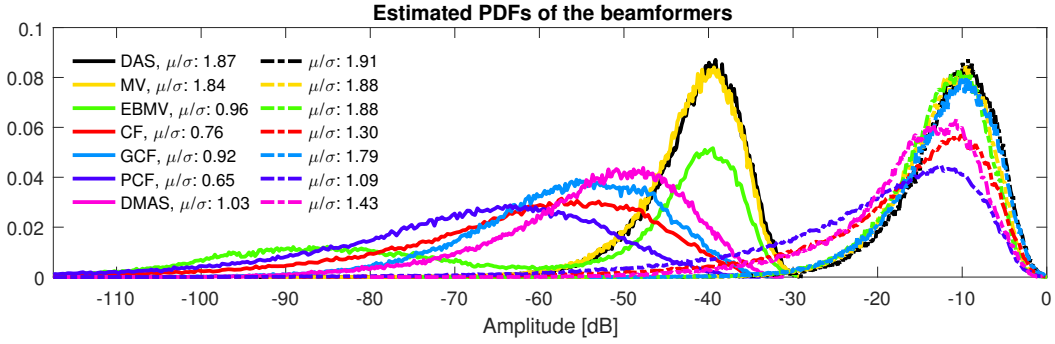

(b) Estimated PDF of dB-scaled image data, horizontal orientation

Fig. 3. Estimated PDFs of the log-compressed images for each speckle region, shown for all beamformers. When the speckle regions are in horizontal orientation, the statistics of the low intensity region is altered compared to the high intensity region.

much lower SNR values. However, for the low intensity region presented in Fig. 2b, only the DAS and MV beamformers are Rayleigh distributed with SNR close to 1.91. The SNR values for the EBMV and GCF beamformers are significantly lower for the low intensity region than the high intensity region. This signifies that the beamformers alter the statistics of the two regions differently. For the CF and PCF beamformers, the SNR was much lower than 1.91 in both cases.

Fig. 3 shows the estimated PDFs of the beamformed log-compressed images for both phantom orientations. When the speckle regions are orientated one on top of the other, i.e. vertical phantom orientation, the speckle statistics for each region within the same image are similar. However, when the speckle regions are horizontally oriented, several of the adaptive beamformers have different distributions for the two regions. The CF, PCF and DMAS beamformers, which had distributions far from theoretical Rayleigh in Fig. 2, have heavy left-tailed distributions for both phantom orientations. However, for the horizontally oriented phantom there is a clear difference between the low intensity region (solid line) and the

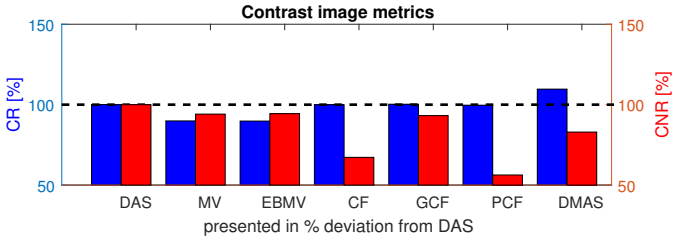

(a) Vertical orientation

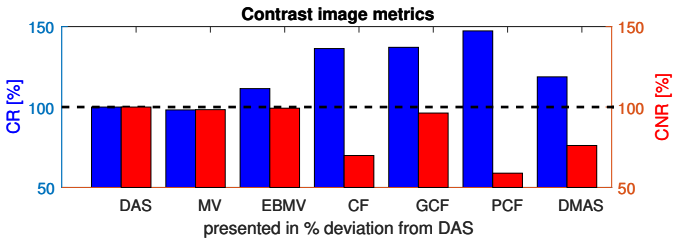

(b) Horizontal orientation

Fig. 4. Contrast metrics for the different adaptive beamformers compared to DAS, given different phantom orientations.

high intensity region (dashed line). The EBMV, CF, GCF and PCF beamformers have much more heavy-tailed distributions for the low intensity region, which corresponds to increased variance. The DMAS beamformer has a deformed PDF for the low intensity region with a second peak emerging at very low intensity.

This leads to the results presented in Fig. 4, where we show that a beamformer may have high CR and simultaneously low CNR compared to DAS. The CR measurements in Fig. 4b indicate that the CF, GCF, PCF and DMAS beamformers have higher contrast than DAS, but concurrently lower CNR compared to DAS. This is consistent with what we observe in Fig. 3 where the EBMV, CF, PCF, GCF and DMAS beamformers have both increased the variance and the intensity difference between the regions. This means that apparent contrast enhancement can be due to alterations of the speckle statistics or the dynamic range. When a beamformer increases the contrast between the speckle regions while also increasing the intensity variance, it is not sufficient to only present one contrast metric when analyzing the beamformer's performance. Presenting only CR as a quality metric would not adequately describe the performance of for example the PCF beamformer when compared to conventional DAS.

The results show that several of the adaptive beamformers are spatially and intensity dependent when altering the speckle statistics of the image data. Further investigation of the intensity dependency should include varying the intensity difference between the regions. Benchmarking the performance of an adaptive beamformer by only using one contrast metric will not sufficiently address any possible spatial or intensity dependent behavior.

VI. Conclusions

We have shown that the effect of adaptive beamformers on the speckle statistics vary for different beamformers. The effect varies also with regard to spatial location of the speckle regions examined. When evaluating a beamformer's performance in comparison to conventional DAS, both the contrast and contrast-to-noise metrics should be presented. Since an adaptive beamformer can alter the speckle statistics, it is imperative that a performance comparison also includes a statistical discussion.

References

[1] O. M. H. Rindal, A. Austeng, H. Torp, S. Holm, and A. Rodriguez-Molares, "The dynamic range of adaptive beamformers," *IEEE International Ultrasonics Symposium, IUS*, no. 1, pp. 1–4, 2016.

[2] O. M. H. Rindal, A. Rodriguez-Molares, and A. Austeng, "The Dark Region Artifact in Adaptive Ultrasound Beamforming," *IEEE International Ultrasonics Symposium, IUS*, 2017.

[3] J.-F. Synnevåg, A. Austeng, and S. Holm, "Adaptive Beamforming Applied to Medical Ultrasound Imaging." *IEEE transactions on ultrasonics, ferroelectrics, and frequency control*, vol. 54, no. 8, aug 2007.

[4] B. M. Asl and A. Mahloojifar, "Eigenspace-based minimum variance beamforming applied to medical ultrasound imaging," *IEEE Transactions on Ultrasonics, Ferroelectrics, and Frequency Control*, vol. 57, no. 11, pp. 2381–2390, 2010.

[5] R. Mallart and M. Fink, "Adaptive focusing in scattering media through sound-speed inhomogeneities: The van Cittert Zernike approach and focusing criterion," *The Journal of the Acoustical Society of America*, vol. 96, no. 6, p. 3721, 1994.

[6] P. C. Li and M. L. Li, "Adaptive imaging using the generalized coherence factor," *IEEE Transactions on Ultrasonics, Ferroelectrics, and Frequency Control*, vol. 50, no. 2, pp. 128–141, 2003.

[7] J. Camacho, M. Parrilla, and C. Fritsch, "Phase coherence imaging," *IEEE Transactions on Ultrasonics, Ferroelectrics, and Frequency Control*, vol. 56, no. 5, pp. 958–974, 2009.

[8] G. Matrone, A. S. Savoia, G. Caliano, S. Member, and G. Magenes, "The Delay Multiply and Sum Beamforming Algorithm in Ultrasound B - Mode Medical Imaging," *IEEE Trans. Med. Imaging*, vol. 34, no. 4, pp. 1–10, 2015.

[9] F. Prieur, O. M. H. Rindal, S. Holm, and A. Austeng, "Influence of the Delay-Multiply-And-Sum beamformer on the ultrasound image amplitude," *IEEE International Ultrasonics Symposium, IUS*, 2017.

[10] J. A. Jensen and N. B. Svendsen, "Calculation of Pressure Fields from Arbitrarily Shaped, Apodized, and Excited Ultrasound Transducers," *IEEE Transactions on Ultrasonics, Ferroelectrics and Frequency Control*, vol. 39, no. 2, pp. 262–267, 1992.

[11] J. A. Jensen, "Field: A Program for Simulating Ultrasound Systems," *Medical & Biological Engineering & Computing*, vol. 34, pp. 351–353, 1996.

[12] A. Rodriguez-Molares, O. M. H. Rindal, O. Bernard, A. Nair, M. A. Lediju Bell, H. Liebgott, A. Austeng, and L. Løvstakken, "The UltraSound ToolBox (USTB)," *IEEE International Ultrasonics Symposium, IUS*, 2017.

[13] D. H.Turnbull, P. K. Lum, A. T. Kerr, and F. S. Foster, "Simulation of B-scan images from two-dimensional transducer arrays: Part I Methods and quantitative contrast measurements," *Ultrasonic Imaging*, vol. 14, no. 4, pp. 323–343, 1992.

[14] M. S. Patterson and F. S. Foster, "The Improvement and quantitative assessment of b-mode images produced by an annular array/cone hybrid," *Ultrasonic Imaging*, no. 5, pp. 195–213, 1983.

[15] R. F. Wagner, S. W. Smith, J. M. Sandrik, and H. Lopez, "Statistics of Speckle in Ultrasound B-Scans," *IEEE Transactions on Sonics and Ultrasonics*, vol. 30, no. 3, 1983.